STEM CELLS AND DEVELOPMENT
Volume 23, Number 19, 2014

DOI: 10.1089/scd.2014.0122

SHIP1 Regulates MSC Numbers and Their Osteolineage Commitment by Limiting Induction of the PI3K/Akt/β-Catenin/Id2 Axis

Sonia Iyer,[1] Dennis R. Viernes,[2] John D. Chisholm,[2] Bryan S. Margulies,[3] and William G. Kerr[1,4]

Here, we show that Src homology 2-domain-containing inositol 5′-phosphatase 1 (SHIP1) is required for the efficient development of osteoblasts from mesenchymal stem cells (MSCs) such that bone growth and density are reduced in mice that lack SHIP1 expression in MSCs. We find that SHIP1 promotes the osteogenic output of MSCs by limiting activation of the PI3K/Akt/β-catenin pathway required for induction of the MSC stemness factor Id2. In parallel, we demonstrate that mice with myeloid-restricted ablation of SHIP1, including osteoclasts (OCs), show no reduction in bone mass or density. Hence, diminished bone mass and density in the SHIP1-deficient mice results from SHIP deficiency in MSC and osteolineage progenitors. Intriguingly, mice with a SHIP-deficient MSC compartment also exhibit decreased OC numbers. In agreement with our genetic findings we also show that treatment of mice with an SHIP1 inhibitor (SHIPi) significantly reduces bone mass. These findings demonstrate a novel role for SHIP1 in MSC fate determination and bone growth. Further, SHIPi may represent a novel therapeutic approach to limit bone development in osteopetrotic and sclerotic bone diseases.

Introduction

Bone undergoes continuous remodeling in the body throughout life. This dynamic process involves a balance between bone-forming osteoblasts (OBs) derived from multipotent mesenchymal stem cells (MSCs) and osteoclasts (OCs) that mediate bone resorption [1]. Studies by Friedenstein and Owen et al. demonstrated that spindle-shaped stromal cells were capable of proliferating and forming colonies [colony forming unit-fibroblasts (CFU-Fs)] that possessed self-renewing capability [2–4]. These spindle-shaped stromal cells, now known as MSCs [5] are a key component of the bone marrow (BM) microenvironment that regulates several key niche functions [6]. In addition, MSCs possess the capacity to self-renew and can differentiate into various cell types including OBs, chondrocytes, adipocytes, or myocytes [7].

Differentiation of uncommitted MSCs into multiple lineages is dependent on several different lineage-associated transcriptional factors. However, the maintenance of MSCs in an uncommitted state is not completely understood. Basic-helix-loop-helix (bHLH) transcription factors perform a wide-array of cellular functions including stem cell commitment [8]. Inhibitor of DNA binding-proteins or inhibitors of differentiation (Ids), which belong to the HLH family of proteins are nuclear factors that lack the basic amino acid region required for DNA-binding [9,10]. Id proteins heterodimerize and sequester bHLH factors, and render them incapable of binding DNA and activating target genes [11–13]. Enforced expression of the Id2 transcription factor has been shown to promote MSC proliferation, while selectively blocking osteolineage differentiation by MSCs [14,15]. The function of Id proteins in maintaining MSCs has recently been shown to require the deubiquitinase USP1, which prevents proteasomal degradation of Id2 [15].

The Src homology 2-domain-containing inositol 5′-phosphatase 1 (SHIP1) regulates cellular processes such as proliferation, differentiation, and survival via the PI3K/AKT pathway. SHIP hydrolyzes the product of PI3K, $PI(3,4,5)P_3$, to generate $PI(3,4)P_2$, which, like $PI(3,4,5)P_3$, can facilitate downstream activation of Akt [16–19]. Previously, others and we have found that HSC from SHIP-deficient mice demonstrate defective repopulating and self-renewal capacity upon transfer to SHIP-competent hosts [20,21]. These findings suggested an intrinsic defect in HSC caused by SHIP deficiency. However, this defect was not observed when HSC were rendered SHIP-deficient in adult hosts where the BM milieu or niche remained SHIP-competent. These findings suggested that defective HSC function in

[1]Department of Microbiology and Immunology, SUNY Upstate Medical University, Syracuse, New York.
[2]Department of Chemistry, Syracuse University, Syracuse, New York.
Departments of [3]Orthopedic Surgery and [4]Pediatrics, SUNY Upstate Medical University, Syracuse, New York.

germline SHIP-deficient hosts might arise from disruption of niche cell components [22]. Consistent with this hypothesis, primary OB were found to express the SH2 domain containing 145 and 150 kDa isoforms encoded by the SHIP1 locus [22]. In addition, BM-derived SHIP1$^{-/-}$ OBs have less alkaline phosphatase (ALP) activity required for bone formation indicating impaired OB development and function [22]. SHIP$^{-/-}$ mutant mice have previously been reported to be osteoporotic [23]. This pathology was attributed to hyperresorptive activity by myeloid-derived OCs [23] resulting from unopposed PI3K signaling at DAP12-associated receptors [24].

Our finding that SHIP1 is expressed by primary OB and that OB development is impaired in germline SHIP$^{-/-}$ mice [22] led us to examine a potential role for SHIP1 in MSC and osteolineage progenitors (MS/PC) function in vivo. Here, we show that SHIP1 is required for the efficient development of OBs from MS/PC such that normal body growth and bone formation rate are impaired in mice that lack expression of SHIP1 in MS/PC. In addition, we show that in the absence of SHIP1 expression MS/PC are biased toward an adipogenic fate. Moreover, SHIP-deficiency promotes a profound expansion of MSC that are selectively hindered for osteolineage commitment due to dysregulation of the PI3K/Akt/GSK3β pathway that promotes nuclear translocation of β-catenin and its induction of the MSC stemness factor Id2. Together, these findings provide a cellular and molecular basis for SHIP1's regulation of MSC numbers in the BM and their osteolineage commitment.

Materials and Methods

Mice and genotyping

SHIP$^{flox/flox}$ mice backcrossed to a C57BL6/J background express normal levels of SHIP, but the SHIP proximal promoter and first exon are floxed, meaning that SHIP can be deleted when Cre recombinase is expressed [25]. Previously described OsxCre [26] and LysMCre [27] transgenic mice were purchased from Jackson Laboratory. Col1a1Cre [28] was purchased from Mutant Mouse Regional Resource Center (MMRRC) at UC Davis. Genotyping of Cre transgenic mice was performed by polymerase chain reaction using primers detecting the *Cre* sequence (P1, 5′-GTGAAA CAGCATTGCTGTCACTT-3′; P2, 5′-GCGGTCTGGCAG TAAAAACTA-3′). The SUNY Upstate Medical University Committee for Humane Use of Animals approved all animal experiments.

Derivation of bone marrow-derived MSC and monocytes

The adherent cell-fraction (MSC) and nonadherent cell-fraction (monocytes) were collected from OSXCreSHIP$^{flox/flox}$ mouse BM and subsequently used to study regulation of the differentiation and metabolic activity of bone cells (OBs, adipocytes, and OCs). Mice were euthanized; femurs and tibia were removed aseptically and flushed using alpha minimum essential medium (αMEM) (Cellgro, Mediatech) and passed through a 70-μm filter into a collection tube. The cells were then resuspended and plated in growth media: αMEM, 10% fetal bovine serum (FBS; Atlanta Biological), 1% penicillin–streptomycin solution (Cellgro, Mediatech), and 1% L-glutamine (Cellgro, Mediatech) and cultured at 37°C with 5% CO_2. After 48 h monocytes were removed and cultured separately for differentiation of OCs. The remaining MSCs were expanded through the third passage for 3–5 weeks and used to assess osteogenic and adipogenic differentiation.

Osteogenic, adipogenic, and OC differentiation

MSCs were induced to become OBs using osteogenic induction media (OIM) or adipogenic induction media (AIM). OIM was composed of β-glycerol 2-phosphate (BGP, 4 mM, Cat: G9891; Sigma) and 2-phospho-L-ascorbic acid (25 μg/mL, Cat: A8960; Sigma) for 14 days, with media changed every 2 days. To assay for formation of mineral nodules, plates were stained with 1% Alizarin red S solution (pH 4.2) [29]. For inhibitor studies, these cells were pretreated for 1 h prior to induction with β-catenin inhibitor, CCT031374 [30] at 20 μM concentration and PI3K/mTOR inhibitor, NVP-BEZ235 at 10 nM concentration [31] respectively. For adipocyte differentiation cells were induced with AIM containing 1 μM dexamethasone, 10 μg/mL insulin, 0.5 mM methylisobutylxanthanine, 5 mM troglitazone, and 10% FBS in αMEM. Adipocytes were stained with Oil Red O as follows: cells were washed with 60% isopropanol and then stained with a 0.35 g/mL Oil Red O solution in isopropanol. Cells were incubated for 10 min with Oil Red working solution and rinsed four times. OCs were differentiated from monocytes cultured for 48 h with 100 ng/mL of recombinant macrophage colony-stimulating factor (M-CSF) (Wyeth). Bone marrow-derived monocytes (BMM) expanded through M-CSF treatment were then cultured (1×10^6 cells/well) with 25 ng/mL recombinant receptor activator of nuclear factor kappa-B ligand (RANKL) (R&D Systems) and 25 ng/mL M-CSF for ~14 days, with media changes every 2 days. Multinucleate OCs were stained with the tartrate-resistant acid phosphatase (TRAP) (Acid Phosphatase, Leukocyte Kit; Sigma) [29]. Multinucleate, TRAP-positive OCs were subsequently counted using a modification of Cavalieri's sampling method and the fractionator to generate an unbiased estimate of the numbers of OCs within each tissue-culture well [32,33]. OCs were also used to detect SHIP expression by western blot.

Western blot analysis

Cell lysates were individually treated and prepared from primary BM-derived cells. Lysate supernatants were resolved on a 7.5% Bis-Tris gel and transferred to a Hybond-ECL nitrocellulose membrane (GE Healthcare). For chemiluminescence the membranes were incubated with specific primary antibodies against SHIP1 (P1C1), Actin, and Id2 (C-20) (Santa Cruz Biotechnology). PTEN, AKT, p-AKT (Ser473), p-GSK3α/β, GSK3β, Id2, and USP1 were purchased from Cell Signaling Technology, Inc. The membrane was blocked with 5% bovine serum albumin or 5% nonfat dry milk in TBS with 0.1% Tween-20 (TBS-T) and probed with specific primary antibody and then by horseradish peroxidase-conjugated secondary antibody (Cell Signaling Technology, Inc.). Protein was detected using Super Signal ECL Substrate/Pico Substrate (Pierce).

CFU-F assay

Primary whole BM cells (adherent + nonadherent) were plated in 60-mm plates (triplicates, 3×10^6 cells/plate) in CFU-F

growth media: αMEM, Mesencult Serum (Stem Cell Technologies) with 1% penicillin–streptomycin–glutamine. Cells were cultured for ~12 days, after which cells were fixed with 70% ethanol and stained for ALP activity using the Leukocyte Alkaline Phosphatase Kit (Sigma) and counter-stained with neutral red (Sigma). ALP^+ cells/colonies stain purple while ALP^- cells/colonies stain red. Colonies were counted when they contained 25 cells per colony using the Software program ''Image J'' (National Institutes of Health Research Services Branch; http://rsbweb.nih.gov/ij/). CFU-F assay was conducted on age-matched male and female $LysMCreSHIP^{flox/flox}$ mice.

Bone mineral apposition rate measurement

Animals were injected with oxytetracycline (OTC; 10 mg/kg) 24h prior to euthanasia. The formalin-fixed bone samples were decalcified using an EDTA-sucrose solution before being embedded in optimum cutting temperature (OCT) compound (Tissue-Tek; Sakura Finetek) and stored at −80°C prior to cryosectioning. Sections were imaged and the mineral apposition rate (MAR) was calculated by measuring the distance from the OTC band to the endosteal surface using the software program ''Image J'' (National Institutes of Health Research Services Branch; http://rsbweb.nih.gov/ij/). Measurements were conducted on age-matched male and female $SHIP^{flox/flox}$ and $OSXCreSHIP^{flox/flox}$ mice.

Bone mass measurements by dual-energy X-ray absorptiometry

Bone mineral density (BMD, g/cm^2), bone mineral content (BMC, grams), and body fat percent were assessed with dual-energy X-ray absorptiometry (DEXA) using a PixiMus scanner (GE Healthcare), according to previously published techniques [34]. Briefly, mice were anesthetized using 5% isoflurane and oxygen. BMD, BMC, and body fat percent was determined using the PixiMus software by identifying a region of interest (excluding the head).

Micro computed tomography

High-resolution images of the tibia were acquired by using a desktop microtomographic imaging system (Micro-CT40; Scanco Medical). The tibia was scanned at 45 keV with an isotropic voxel size of 6 μm, and the resulting two-dimensional cross-sectional images are shown in grayscale. Proximal tibial scans were conducted to capture the same region of the metaphysis independent of gender or age, such that the number of slices selected for scanning began at the most proximal aspect of the tibia and extended a distance equal to 20% of the length of the tibia. In addition, a mid-shaft diaphyseal scan of 50 slices was conducted using the midpoint landmark tool present in the Scanco analysis software. In both cases a series of axial images was produced; however, proximal tibial images were resampled to be sagittal for analysis. Metaphyseal bone volume over tissue volume (Bv/Tv) was calculated using the Scanco software, within a 50-slice region of interest centered on the central long-axis of the tibia and bounded by the growth plate at the proximal end and an arbitrary 1.5 mm point distal to the growth plate, with cortical bone carefully excluded. Metaphyseal thickness was determined using unbiased stereology, in which a ''thickness'' was measured in individual sections spaced 5 μm apart through the primary and second spongiosa [35].

Nile Red staining

To directly assay the BM fat compartment, tibias were fixed using 10% neutral-buffered formalin, snap-frozen, and then sectioned at 10 μm. Sections were then stained for adiposity with 12 mg/mL of the lipophilic fluorescent stain Nile Red (Sigma) and counterstained with 10 μg/mL 4′,6-diamidino-2-phenylindole (DAPI; Sigma) for morphology.

Histomorphometric analysis of proximal tibial growth plate

The formalin-fixed bone samples were decalcified using an EDTA-sucrose solution before being embedded in OCT compound (Tissue-Tek; Sakura Finetek) and stored at −80°C prior to cryosectioning. Total growth plate, proliferative zone, and hypertrophic zone heights were measured as described in [35].

TRAP staining of proximal tibia sections

The formalin-fixed bone samples were decalcified using an EDTA-sucrose solution before being embedded in OCT compound (Tissue-Tek; Sakura Finetek) and stored at −80°C prior to cryosectioning. To identify OCs TRAP staining was performed using the Acid Phosphatase, Leukocyte Kit (Sigma) and counterstained using an acidified 1% methyl green.

Hematologic analysis

Peripheral blood samples were harvested in EDTA-coated microtubes (Sarstedt Co.) by submandibular bleeding and analyzed with a HEMAVET 950S Veterinary Hematology Analyzer (Drew Scientific, Inc.) using the mouse species program.

Ex vivo MSC immunophenotyping by flow cytometry

For FACS phenotyping of MSCs, BM-derived MSCs were seeded in quadruplet wells of a 60 mm plate at 1×10^5 cells/well. When the cells reached 80%–90% confluency osteogenesis was induced by the addition of BGP (10 mM, Cat: G9891; Sigma) and 2-phospho-L-ascorbic acid (50 μg/mL, Cat: A8960; Sigma) for 6 days, with osteogenic media changed every other day. Uninduced cells were seeded simultaneously and were used as controls. On day 6, cells were trypsinized and washed twice with staining buffer [3% heat-inactivated FBS, 2.5 mM HEPES in 1× phosphate-buffered saline (PBS)]. 2.5×10^6 cells were treated with CD16/CD32 mouse Fc block (2.4G2) on ice for 15 min and then stained with a panel of antibodies. The Lineage (Lin) panel included endothelial and hematopoietic markers on FITC; CD2 (RM2-5), CD3ε (145-2C11), CD4 (GK1.5), CD5 (53-7.3), CD8α (53-6.7), B220 (RA3-6B2), Gr-1 (RB6-8C5), Mac-1 (M1/70), NK1.1 (PK136), Ter119 (TER-119), CD31 (PECAM-1), CD34 (RAM34), CD45 (30-F11), CD86 (B7-2), MHC Class II (I-A/I-E), and CD43 (R2/60). MSC marker CD29 (Integrin beta 1, clone HMb1-1) was used to positively demarcate MSCs within the Lin-negative cell population. All antibodies were purchased from BD Biosciences and eBioscience.

In vivo MSC immunophenotyping by flow cytometry

PDGFRα^+CD51$^+$ MSC [36] and PDGFRα^+Sca1$^+$ MSC [37] were detected using methods and reagents as described by Winkler et al. [38], Schepers et al. [39], Morikawa et al. [37], Houlihan et al. [40] and Pinho et al. [36]. Femurs, tibias, humeri, ulnas, radii, and pelvis were dissected. The bone fragments after flushing to remove the marrow were then cleaned, cut into 1 cm pieces, and then crushed using a mortar and pestle. The remaining bone chips were then washed several times in HBSS supplemented with 2% heat-inactivated FBS (HBSS/2% HI-FBS) and HBSS only, and then spun at 350 *g* for 5 min. The pellet was resuspended in 3 mg/mL type I collagenase (Worthington) and 15 μg/mL DNAase (Sigma) dissolved in HBSS. The cells were incubated twice for 30 min at 110 rpm and 37°C. Following incubation, mononuclear cells were obtained using a Ficoll gradient (Histopaque-1119 and Histopaque-1077; Sigma), and were then used for further analysis. The cells were resuspended in HBSS/2% HI-FBS and washed twice before staining. Roughly, $2–10\times10^6$ cells were treated with CD16/CD32 mouse Fc block (2.4G2) on ice for 15 min and then stained with the following panel of antibodies: Lineage (Lin) panel included hematopoietic markers on FITC; CD2 (RM2-5), CD3ε (145-2C11), CD4 (GK1.5), CD5 (53-7.3), CD8α (53-6.7), B220 (RA3-6B2), Gr-1 (RB6-8C5), Mac-1 (M1/70), NK1.1 (PK136), Ter119 (TER-119), and CD45 (30-F11). The other markers include APC-CD31 (390), PE-Cy7-Sca-1 (D7), Biotin-CD140a (PDGF Receptor α) (APA5), and PE-CD51 (RMV-7). A second step stain with Streptavidin-APC-Cy7 was used to reveal staining with the biotin-conjugated CD140a Ab. Dead cells were excluded from postcollection analysis using DAPI.

Annexin V staining

Apoptotic MSCs were evaluated on day 6 of osteogenic induction as described above. 2.5×10^5 cells were treated with CD16/CD32 mouse Fc block (2.4G2) on ice for 15 min and stained with Lin panel and the MSC marker CD29 on ice for 30 min. Cells were washed once with cold PBS, resuspended in 1× binding buffer, and stained with APC-labeled Annexin V for 15 min at room temperature, protected from light. Cells were washed once and resuspended in 200 μL of 1× binding buffer. The frequency of Annexin V$^+$ within the CD29$^+$Lin$^-$ MSC populations were detected and quantitated by flow cytometry.

Use of SHIPi (3AC) for in vivo studies

SHIP1 inhibitor (SHIPi) in the form of 3-a-aminocholestane (3AC) was administered intraperitoneally at 25 mg/kg of body weight as published earlier [19]. Vehicle-treated mice received 100 μL injection of 0.3% Klucel/H_2O solution. Six to 12-months-old C57BL6/J mice were treated with SHIPi or vehicle three times per week for 4, 8, and 12 weeks.

Bone mechanical testing

Mouse femurs were cleaned, wrapped in PBS-soaked gauze, and frozen at −20°C. Femurs were rehydrated in a PBS solution at room temperature for 2 h before testing. We employed a three-point-bending test to assay the biomechanical properties of femurs treated with SHIPi. Femurs were placed into a testing frame (1250 N Load Cell and a Q Test 1/L; MTS Systems Corp), preloaded with 1 N, and then loaded at 1 N/mm until failure. Prior to testing, femurs were scanned using micro computed tomography (microCT) to assay the geometric properties.

Statistical analysis

All statistical analyses were performed using the statistical software Prism (GraphPad). Body weight was assayed using analysis of covariance while MAR, Bv/Tv, metaphyseal thickness, TRAP numbers, CFU-F measurements, BMD, BMC, and %body fat (assayed with DEXA) were all analyzed using Student's *t*-test with a $P<0.05$. Ex vivo tissue culture differentiation experiments (CFU-F, osteogenesis, adipogenesis, and osteoclastogenesis) were performed with three replicates in each experiment with each experiment performed a minimum of three times. Flow cytometry experiments were analyzed using Student's *t*-test with a $P<0.05$.

Results

Mice with ablation of SHIP1 in MS/PC exhibit impaired growth and an expanded MSC compartment

We previously found that BM stromal cells enriched for MS/PC express SHIP1 and the OB compartment in SHIP1$^{-/-}$ mice exhibits impaired maturation [22]. We hypothesized then that SHIP1 might play a cell intrinsic role in the ability of the MS/PC compartment to generate mature OB and thus bone growth. To test this we developed mice harboring a floxed SHIP locus [25] combined with a Cre recombinase transgene under the control of the Osterix promoter that enables selective deletion in preosteoblastic mesenchymal stem/progenitors [26,41]. We first confirmed ablation of SHIP1 expression in MS/PC prepared from adult OSXCreSHIP$^{flox/flox}$ mice by western blot analysis of lysates from MS/PC cultured in a primitive, uninduced state and following induction of osteogenic differentiation (Fig. 1A). This analysis confirmed that SHIP1 is expressed by MS/PC (see *SHIP*$^{flox/flox}$ lanes). Importantly, we observed no ablation of SHIP1 expression in circulating peripheral blood mononucleated cells (PBMC) (Fig. 1B) or BM-derived OCs obtained from multiple OSXCreSHIP$^{flox/flox}$ mice (Fig. 1C), confirming that SHIP1 expression in the hematopoietic compartment and myeloid-derived OC remains intact in OSXCreSHIP$^{flox/flox}$ mice. Adult OSXCreSHIP$^{flox/flox}$ mice are viable; however, we observed a significant under-representation of OSXCreSHIP$^{flox/flox}$ weanlings versus their expected Mendelian frequency ($P<0.0001$, binomial exact test) (Supplementary Table S1), indicating a survival disadvantage for fetuses and/or neonates that lack mesenchymal stem/progenitor expression of SHIP. However, OSXCreSHIP$^{flox/+}$ mice are born and weaned at a normal Mendelian ratio. Despite normal postweaning viability, the loss of SHIP1 in OSXCreSHIP$^{flox/flox}$ mice resulted in profound effects on their growth. Although male and female OSXCreSHIP$^{flox/flox}$ mice were indistinguishable in size at birth from their SHIP$^{flox/flox}$ counterparts, OSXCreSHIP$^{flox/flox}$ mice were smaller at the time of weaning and remain smaller

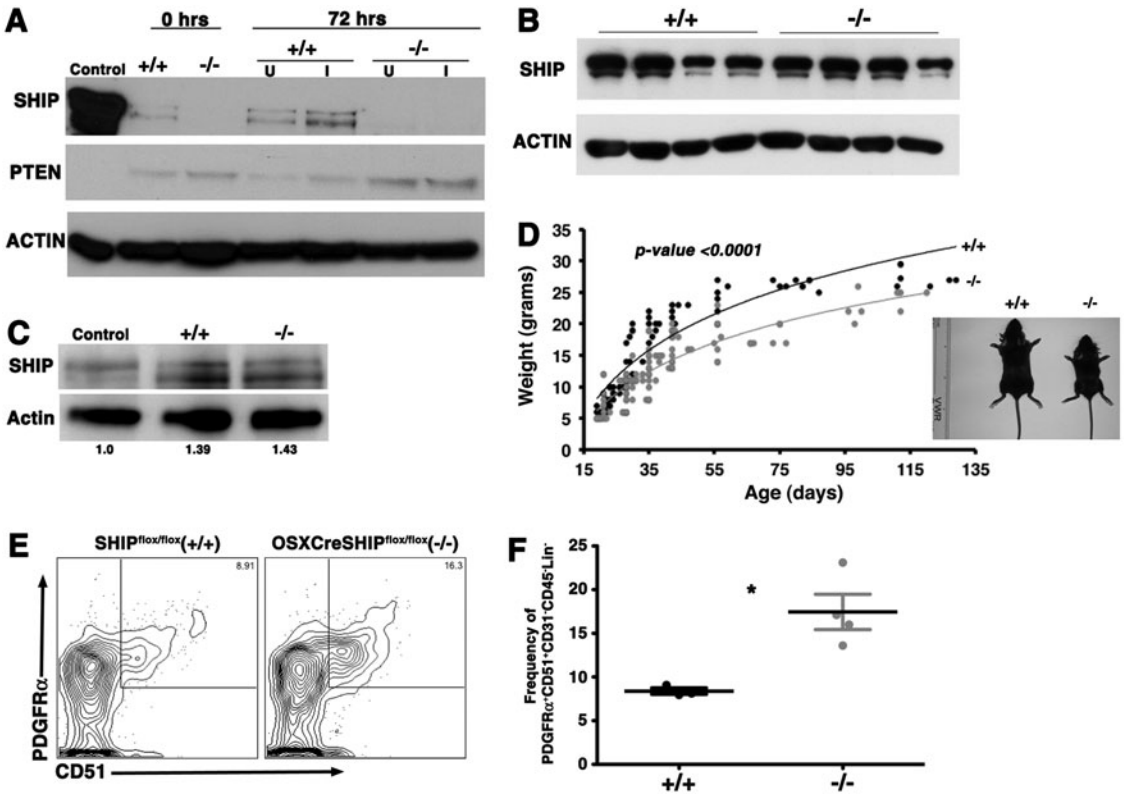

FIG. 1. MSC and osteolineage progenitors (MS/PC)-specific ablation of Src homology 2-domain-containing inositol 5′-phosphatase 1 (SHIP1) expression retards growth and expanded mesenchymal stem cell (MSC) compartment. **(A)** Bone marrow (BM)-derived MSCs were cultured in conditions that induce osteoblast (OB) differentiation. SHIP1 and PTEN expression in cell lysates were assessed by immunoblotting at days 0 and 3. Actin serves as a loading control. *Lanes* containing $SHIP^{flox/flox}$ (+/+) or $OSXCreSHIP^{flox/flox}$ (−/−) cell lysates are as indicated. **(B)** SHIP1 level in blood mononuclear cell lysates were assessed by immunoblotting from four independent $SHIP^{flox/flox}$ (+/+) and $OSXCreSHIP^{flox/flox}$ (−/−) mice. **(C)** Macrophage progenitors in BM were cultured with RANKL and M-CSF and SHIP1 levels in whole cell lysates (WCL) were assessed by immunoblotting at day 3 of differentiation. Actin quantification was performed using Image lab software 3.0.1 Beta 2; Bio-Rad Laboratories. *Lanes* containing control (WT), $SHIP^{flox/flox}$ (+/+) or $OSXCreSHIP^{flox/flox}$ (−/−) cell lysates are as indicated. **(D)** Weights of male $SHIP^{flox/flox}$ (*black circles*) and $OSXCreSHIP^{flox/flox}$ (*gray circles*) mice, each symbol represents an individual mouse, between 19 and 129 days postpartum, data analysis was performed using analysis of covariance (ANCOVA) followed by Bonferroni's multiple comparison post hoc test with age or gender to evaluate the differences between groups. Representative images of 3-week-old male $SHIP^{flox/flox}$ (+/+) and $OSXCreSHIP^{flox/flox}$ (−/−) (see *inset*). **(E)** Representative contour plots of $PDGFR\alpha^+51^+$ MSC ($PDGFR\alpha^+CD51^+CD31^-CD45^-Lin^-$) in 8–10-week-old $SHIP^{flox/flox}$ (+/+) and $OSXCreSHIP^{flox/flox}$ (−/−) mice. **(F)** Bar graph of $P\alpha^+51^+$ MSC frequency among $CD31^-CD45^-Lin^-$ cells in $OSXCreSHIP^{flox/flox}$ (−/−) versus $SHIP^{flox/flox}$ controls (+/+) ($n=4$), ± SEM. $^*P \le 0.05$, Student's unpaired, two-tailed *t*-test). Note: significant difference in weight was also observed in age-matched female $SHIP^{flox/flox}$ and $OSXCreSHIP^{flox/flox}$ littermates. RANKL, receptor activator of nuclear factor kappa-B ligand.

throughout life. This growth retardation was confirmed by measuring body weight weekly (Fig. 1D and Supplementary Fig. S1A). In Figure 1D we show images of representative 3-week-old male littermates of $OSXCreSHIP^{flox/flox}$ and $SHIP^{flox/flox}$, mice in which the former exhibit distinct growth retardation relative to their SHIP1-competent $SHIP^{flox/flox}$ littermates. We observed no difference in the body weight of $OSXCreSHIP^{flox/+}$ mice in comparison to $SHIP^{flox/flox}$ age and gender-matched controls (Supplementary Fig. S1B; Supplementary Data are available online at www.liebertpub.com/scd). Thus, expression of Cre recombinase from the Osterix promoter does not alter the growth or viability of mice.

As SHIP1 has been previously shown to limit HSC frequency in vivo [20] we then sought to determine whether SHIP1 might play a comparable role in control of MSC homeostasis in vivo. Thus, we analyzed the frequency of MSC by two well-validated phenotypes where single cell cloning assays have confirmed that these cell populations are highly enriched for multipotent cells capable of self-renewal [36]. Multi-parameter flow cytometry analysis showed that MSC of the $PDGFR\alpha^+CD51^+CD31^-CD45^-Lin^-$ phenotype (Fig. 1E, F) or the $PDGFR\alpha^+Sca1^+CD31^-CD45^-Lin^-$ phenotype (Supplementary Fig. S2A, B) are both significantly increased in $OSXCreSHIP^{flox/flox}$ mice as compared with $SHIP^{flox/flox}$ controls. Thus, SHIP1 limits MSC numbers in vivo; however, the negative impact of its ablation in the MS/PC compartment on body mass and size noted above suggested that these expanded MS/PC might have altered developmental properties.

Mice with a SHIP1-deficient MS/PC compartment exhibit impaired bone growth

The decreased body size and mass that we observed in OSXCreSHIP$^{flox/flox}$ mice are consistent with impaired bone formation by MSC. Thus, we directly assessed several independent parameters of bone growth in OSXCreSHIP$^{flox/flox}$ mice and SHIP1-sufficient SHIP$^{flox/flox}$ and OSXCreSHIP$^{flox/+}$ controls. Direct evidence for impaired bone formation and growth in OSXCreSHIP$^{flox/flox}$ mice was provided by analysis of bone mineral apposition rate (MAR), DEXA analysis and three-dimensional microCT. The bone MAR in OSXCreSHIP$^{flox/flox}$ mice is less than half of that observed in SHIP1-sufficient SHIP$^{flox/flox}$ controls (Fig. 2A, B). Whole body BMD and BMC of OSXCreSHIP$^{flox/flox}$ mice, as measured by DEXA, was also significantly reduced relative to SHIP$^{flox/flox}$ controls in both young adult (6–10 weeks of age) and older adults (4–5 months of age) (Fig. 2C, D). Although we see reduced total body BMC by DEXA in the OSXCreSHIP$^{flox/flox}$ mice in comparison to SHIP$^{flox/flox}$ controls, we did not observe any reduction in mineralization as would be consistent with an osteomalacial or rickets phenotype (data not shown). To control the potential impact of Cre expression on OB development we also analyzed OSXCreSHIP$^{flox/+}$ mice by DEXA.

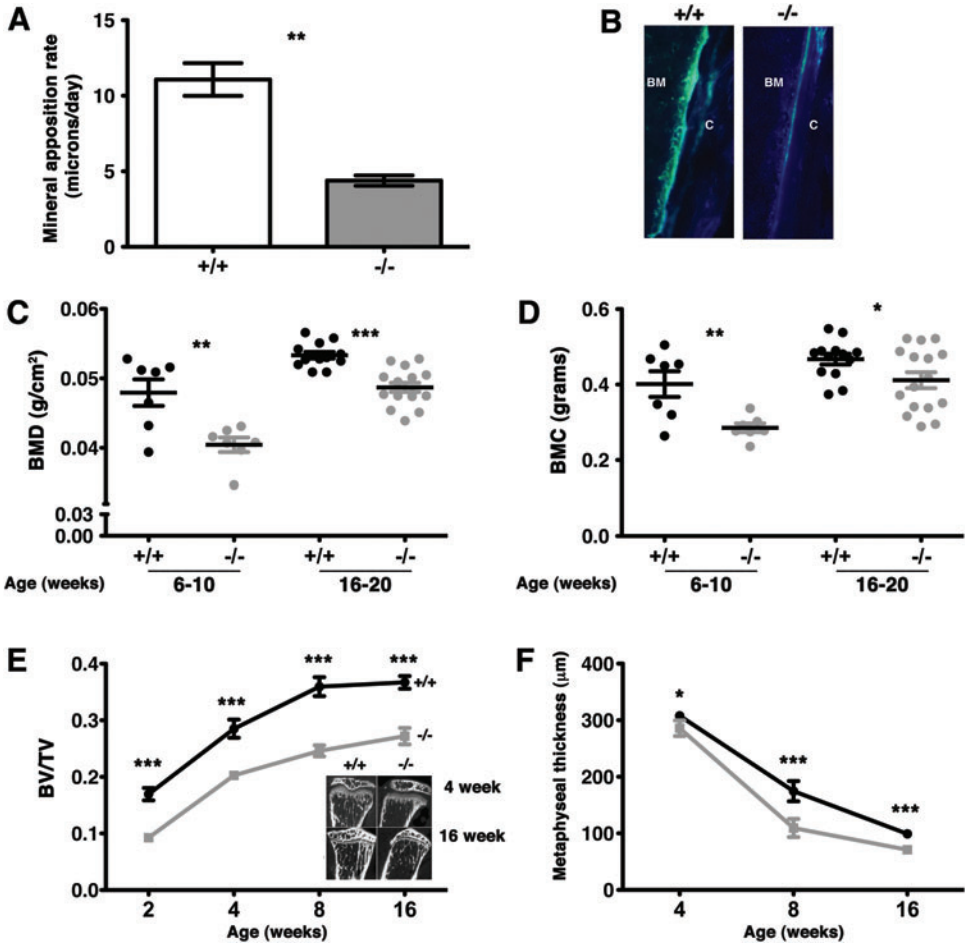

FIG. 2. A SHIP-deficient MS/PC compartment limits bone apposition and causes osteoporosis. Mineral apposition rate (MAR) was calculated by measuring the distance from the oxytetracycline band to the endosteal surface. **(A)** Reduced bone MAR was observed in 3-week-old OSXCreSHIP$^{flox/flox}$ in comparison to SHIP$^{flox/flox}$ controls. ($n \geq 4$, ±SEM $^{**}P \leq 0.001$ Student's unpaired, two-tailed *t*-test) **(B)** Representative images of oxytetracycline band seen in SHIP$^{flox/flox}$ (+/+) and OSXCreSHIP$^{flox/flox}$ (−/−) C, cortical bone. **(C)** Whole-body bone mineral density (BMD) and **(D)** bone mineral content (BMC) by DEXA analysis of 6–20-week-old SHIP$^{flox/flox}$ (+/+) and OSXCreSHIP$^{flox/flox}$ (−/−) mice; ($n \geq 7$, ±SEM. $^{*}P \leq 0.05$, $^{**}P \leq 0.001$ and $^{***}P \leq 0.0001$ Student's unpaired, two-tailed *t*-test, each symbol represents an individual mouse). **(E)** Metaphyseal histomorphometric parameters, bone volume over tissue volume (Bv/Tv), measured at 2, 4, 8 and, 16 weeks in SHIP$^{flox/flox}$ (+/+) and OSXCreSHIP$^{flox/flox}$ (−/−) mice (±SEM $^{***}P \leq 0.0001$ Student's unpaired two-tailed *t*-test). Representative micro computed tomography (microCT) scans of sagittal sections through the proximal metaphysis taken from 4- and 16-week-old SHIP$^{flox/flox}$ (+/+) and OSXCreSHIP$^{flox/flox}$ (−/−) mice (*inset*). **(F)** Metaphyseal thickness (μm) of 4, 8, and 16 week-old-male SHIP$^{flox/flox}$ (+/+) (*black circles*) and OSXCreSHIP$^{flox/flox}$ (−/−) (*gray squares*) mice (±SD $^{*}P \leq 0.05$ and $^{***}P \leq 0.0001$ Student's unpaired, two-tailed *t*-test). Significant difference in metaphyseal thickness was also observed in female SHIP$^{flox/flox}$ and OSXCreSHIP$^{flox/flox}$ littermates. Note: results presented for MAR, BMC, and Bv/Tv represent pooled male and female SHIP$^{flox/flox}$ and OSXCreSHIP$^{flox/flox}$ mice. Color images available online at www.liebertpub.com/scd

No difference in BMD or body weight was observed between OSXCreSHIP$^{flox/+}$ and SHIP$^{flox/flox}$ age and gender-matched controls in either parameter (Supplementary Fig. S1C). In addition, analysis by microCT showed that OSXCreSHIP$^{flox/flox}$ mice have diminished bone mass (Bv/Tv) within the proximal tibial metaphysis (Fig. 2E). Consistent with decreased Bv/Tv in the tibial metaphysis, we also find that metaphyseal thickness is decreased in OSXCreSHIP$^{flox/flox}$ mice relative to SHIP$^{flox/flox}$ controls (Fig. 2F). Thus, the in vivo analysis of bone growth and mineral content by DEXA and microCT demonstrate that the osteoblastic output of SHIP1-deficient MS/PC compartment in OSXCreSHIP$^{flox/flox}$ mice is significantly impaired. This represents the first demonstration that SHIP1 plays an intrinsic role in the function of MS/PC.

The MS/PC compartment is expanded in OSXCreSHIP$^{flox/flox}$ mice, but exhibits altered osteogenic, chondrogenic, and adipogenic output

SHIP is required for normal OB development and we compared osteogenic differentiation between MS/PC from OSXCreSHIP$^{flox/flox}$ mice and SHIP$^{flox/flox}$ controls using Alizarin red staining for mineral deposition in vitro. Differentiated OSXCreSHIP$^{flox/flox}$ MS/PC showed significantly reduced mineralization upon induction of osteogenic differentiation compared with control SHIP$^{flox/flox}$ OB (Fig. 3A). In parallel, we also assessed the ability of MSC cultures derived from OSXCreSHIP$^{flox/flox}$ mice to differentiate into adipocytes ex vivo. Intriguingly, we find more adipocytic cells are obtained from OSXCreSHIP$^{flox/flox}$

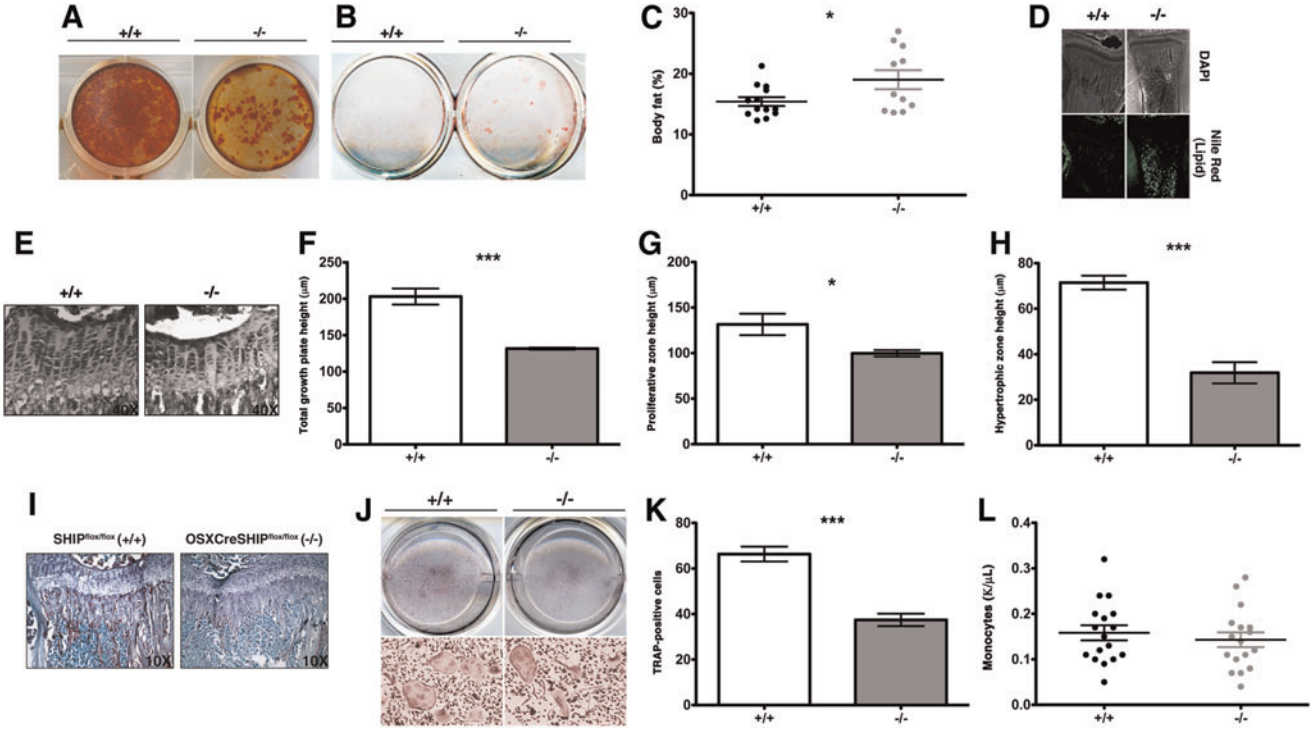

FIG. 3. SHIP deficiency in MS/PC causes defective development of osteolineage cells, growth plate chondrocytes, causes enhanced adipogenesis, and defective development of osteoclastogenesis. **(A)** Alizarin red staining after osteogenic induction of MSC from OSXCreSHIP$^{flox/flox}$ mice $(-/-)$ in comparison to SHIP$^{flox/flox}$ $(+/+)$ at 4 weeks of age ($n=5$). **(B)** Oil Red-O staining on day 21 in OSXCreSHIP$^{flox/flox}$ $(-/-)$ in comparison to SHIP$^{flox/flox}$ $(+/+)$ after adipocyte induction of MSC at 4 weeks of age ($n=5$). **(C)** Body fat between 6 and 10 weeks in OSXCreSHIP$^{flox/flox}$ $(-/-)$ in comparison to SHIP$^{flox/flox}$ $(+/+)$ controls ($n \geq 10, \pm$ SEM. $^*P \leq 0.05$ Student's unpaired, two-tailed t-test, each symbol represents an individual mouse, data represent pooled male and female SHIP$^{flox/flox}$ and OSXCreSHIP$^{flox/flox}$ mice). **(D)** Nile Red (*green*) fluorescent staining of the BM of 4-week-old OSXCreSHIP$^{flox/flox}$ $(-/-)$ and SHIP$^{flox/flox}$ tibias $(+/+)$; DAPI staining (*top panels*) was employed to observe general morphology ($4\times$ magnification). **(E)** Representative images of the growth plates of OSXCreSHIP$^{flox/flox}$ $(-/-)$ and SHIP$^{flox/flox}$ $(+/+)$ control mice, $40\times$ magnification image. **(F)** Total growth plate, **(G)** proliferative zone, and **(H)** hypertrophic zone height of OSXCreSHIP$^{flox/flox}$ $(-/-)$ and SHIP$^{flox/flox}$ $(+/+)$ control mice ($n=4$ mice, $\pm$ SEM. $^*P \leq 0.05$ and $^{***}P \leq 0.0001$, Student's unpaired, two-tailed t-test). **(I)** TRAP$^+$ osteoclasts (OCs) observed in the proximal tibia sections of OSXCreSHIP$^{flox/flox}$ $(-/-)$ and SHIP$^{flox/flox}$ $(+/+)$ controls, in the metaphysis ($10\times$ magnification). **(J)** TRAP staining of OCs differentiated from bone marrow-derived monocytes (BMM) in the presence of RANKL and M-CSF in 8-weeks-old BM of OSXCreSHIP$^{flox/flox}$ $(-/-)$ and SHIP$^{flox/flox}$ $(+/+)$ control mice. *Top panels* are from representative plates and the *bottom panels* are $10\times$ magnifications from these plates. **(K)** The corresponding quantitation of TRAP$^+$ OCs shown to the right SHIP$^{flox/flox}$ $(+/+)$ and OSXCreSHIP$^{flox/flox}$ $(-/-)$, ($n=6$ mice, $\pm$ SEM. $^{***}P \leq 0.0001$, Student's unpaired, two-tailed t-test). **(L)** Circulating monocyte in peripheral blood measured in OSXCreSHIP$^{flox/flox}$ $(-/-)$ and SHIP$^{flox/flox}$ $(+/+)$ controls. Color images available online at www.liebertpub.com/scd

MSC than SHIP$^{flox/flox}$ MSC (Fig. 3B). Consistent with ex vivo analysis of adipogenic differentiation by SHIP1-deficient MS/PC, we also find that the systemic % total body fat (Fig. 3C) and BM (metaphyseal) fat content (Fig. 3D) is significantly increased in OSXCreSHIP$^{flox/flox}$ mice, confirming MS/PC lineage commitment is skewed in vivo. We also examined the proximal tibial growth plates in OSXCreSHIP$^{flox/flox}$ and SHIP$^{flox/flox}$ mice (Fig. 3E) using a histomorphometric analysis of growth plate heights, proliferative zone heights, and hypertrophic zone heights [35]. We observed a decrease in the height of the total growth plate (Fig. 3F), proliferative zone (Fig. 3G), and hypertrophic zone (Fig. 3H) that reflects the decrease in the limb length [42]. Growth plate chondrocyte proliferation is driven in part through the well-known feedback loop, in which reserve zone chondrocytes produce parathyroid hormone-related peptide (PTHrP) that prevents chondrocyte differentiation [43]. As the gradient of PTHrP decreases hypertrophic chondrocytes express factors that drive proliferation in the proliferative zone of the growth plate [44]. The inability of proliferating chondrocytes to differentiate into hypertrophic chondrocytes parallels our observation that preosteoblasts are unable to differentiate into mature OBs, resulting in significant loss of accumulated bone mass.

MS/PC expression of SHIP1 is required for normal osteoclastogenesis

SHIP deficiency in one cell type can lead to lineage extrinsic effects on other lineages that alter their homeostasis and function [22,45]. There is a considerable body of evidence that immature OB promote the differentiation of OCs and that function of the OB lineage is also critical for bone homeostasis and remodeling [46–49]. Thus, we examined the number of OC present in the BM of OSXCreSHIP$^{flox/flox}$ mice versus SHIP$^{flox/flox}$ controls using both ex vivo and an in vivo TRAP staining (Fig. 3I–K). Consistent with an impaired ability of SHIP1-deficient MS/PC to commit to the OB lineage we observed drastically decreased numbers of TRAP$^+$ OC in vivo in OSXCreSHIP$^{flox/flox}$ bone when compared with SHIP$^{flox/flox}$ controls (Fig. 3I). This in situ analysis of OC frequency was confirmed by analysis of OC differentiation of BMM cells from both genotypes ex vivo (Fig. 3J, K). As expected this is not a pan-myeloid effect, since impaired osteolineage commitment by SHIP1-defcient MS/PC did not adversely affect circulating monocyte numbers in the peripheral blood (Fig. 3L). Therefore, the intrinsic impact of SHIP1 deficiency on the mesenchymal compartment adversely impacts OB commitment and differentiation, and consequently also has a lineage extrinsic impact on OC maturation.

SHIP1 expression represses Id2 to facilitate osteolineage commitment and limit proliferation of MSC

We noted that BM-derived MSC cultures from OSXCreSHIP$^{flox/flox}$ mice showed significantly increased total cell numbers both prior to and after induction of osteogenic differentiation. We analyzed these MSC cultures by flow cytometry to determine whether the increased cell number reflected a greater degree of proliferation and survival by OSXCreSHIP$^{flox/flox}$ MSC. We quantified the frequency and absolute numbers of MSC in these cultures using the CD29$^+$Lin$^-$ MSC phenotype recently described by Zhu et al. [50] (Fig. 4A–C). The numbers of MSC was significantly higher in the OSXCreSHIP$^{flox/flox}$ cultures relative to SHIP$^{flox/flox}$ MSC cultures indicating SHIP-deficient MSC proliferate at a higher rate and resist differentiation even under osteogenic culture conditions (Fig. 4C). In fact, the absolute yield of MSCs derived from OSXCreSHIP$^{flox/flox}$ BM is $\sim$10-fold higher indicating a profound expansion of MSC. In addition to having a growth advantage, SHIP1-deficient MSCs ex vivo were not found to be more susceptible to apoptosis (based on reduced Annexin V staining) than SHIP-competent MSCs (Fig. 4D, E). We then hypothesized that SHIP1 signaling limits the activation of the distal signaling components that promote the survival and

FIG. 4. Dysregulation of the PI3K/Akt/β-catenin/Id2 axis promotes MSC expansion in vivo and ex vivo. BM MSC from OSXCreSHIP$^{flox/flox}$ (−/−) or SHIP$^{flox/flox}$ (+/+) littermates were seeded at equal numbers and cultured under osteogenic conditions (I) for 5 days and processed as described. Uninduced cells (U) were used as controls for all experiments and were also initially seeded at equal cell numbers. Results shown are representative of three independent experiments for MSC of the indicated genotypes and are representative of MSC cultures prepared from 4- to 16-week-old mice. Flow cytometry gates for **(A)** uninduced and induced cultures (osteogenic conditions) to detect CD29$^+$Lin$^-$ MSC population in cultures prepared from OSXCreSHIP$^{flox/flox}$ (−/−) and SHIP$^{flox/flox}$ (+/+) mice. Cells were gated for: SSC-H versus FSC-H lack of expression of a Lineage marker panel and surface expression of CD29$^+$ as indicated. **(B)** Significant increased frequency of OSXCreSHIP$^{flox/flox}$ (−/−) CD29$^+$Lin$^-$ MSC before (uninduced, U) and after osteogenic induction (induced, I) (±SEM. $^{**}P \le 0.001$ and $^{***}P \le 0.0001$ Student's unpaired, two-tailed *t*-test). **(C)** The absolute numbers of OSXCreSHIP$^{flox/flox}$ (−/−) MSC in both uninduced (U) and induced (I) conditions in OSXCreSHIP$^{flox/flox}$ (−/−) and SHIP$^{flox/flox}$ (+/+) controls. (±SEM. $^{***}P \le 0.0001$, Student's unpaired, two-tailed *t*-test) **(D)** Representative Annexin V histograms for bulk MS/PC prepared from SHIP$^{flox/flox}$ (+/+) *black lines* and OSXCreSHIP$^{flox/flox}$ (−/−) *gray lines* mice cultured under uninduced (U) and osteogenic induction (I) conditions. **(E)** Bar graphs indicating the frequency of apoptotic SHIP$^{flox/flox}$ (+/+) and OSXCreSHIP$^{flox/flox}$ (−/−) CD29$^+$Lin$^-$ MSC during ex vivo culture in the absence or presence of osteogenic induction factors (±SEM. $^{***}P \le 0.0001$ Student's unpaired, two-tailed *t*-test). **(F)** Phosphorylation status of AKT and GSK3α/β in SHIP$^{flox/flox}$ (+/+) and OSXCreSHIP$^{flox/flox}$ (−/−) BM-derived MSC cultures in the absence (U) or presence (I) of osteogenic induction factors. **(G)** Expression of Id2 and USP1, was examined by western blotting with β-actin serving as loading control, in SHIP$^{flox/flox}$ (+/+) and OSXCreSHIP$^{flox/flox}$ (−/−) in the absence (U) or presence (I) of osteogenic induction factors. **(H)** OSXCreSHIP$^{flox/flox}$ (−/−) or SHIP$^{flox/flox}$ (+/+) MSC (U) and were pretreated for an hour with β-catenin inhibitor (CCT031374) and the pan-PI3K/mTOR inhibitor (NVP-BEZ235) prior to osteogenic induction (I). Expression of Id2 was examined by western blotting with β-actin serving as loading control.

proliferation of MSCs at the expense of OB differentiation. Consistent with this hypothesis we find increase in Akt phosphorylation in SHIP-deficient MSCs relative to SHIP1-sufficient controls both prior to and after osteogenic induction (Fig. 4F). Consequently, Akt activity is increased in BM-derived MSCs of OSXCreSHIP$^{flox/flox}$ as confirmed by increased phosphorylation of one of Akt's key targets, GSK3β (Fig. 4F). GSK3β is inactivated by phosphorylation and promotes activation and nuclear translocation of β-catenin. Recent work by Perry et al. showed that β-catenin activation leads to upregulation of Id2 expression that blocks myeloid progenitor differentiation [51]. Western blot analysis for Id2 revealed that SHIP-deficient MSCs express higher levels of protein under undifferentiated growth, but also importantly under osteogenic conditions on a per cell basis (Fig. 4G). Moreover, we saw coordinate overexpression of USP1 as well (Fig. 4G). USP1 is necessary to prevent proteasomal degradation of Id2 and sustains its expression at a level sufficient to promote MSC proliferation and block OB differentiation [15]. Constitutive super-induction of Id2

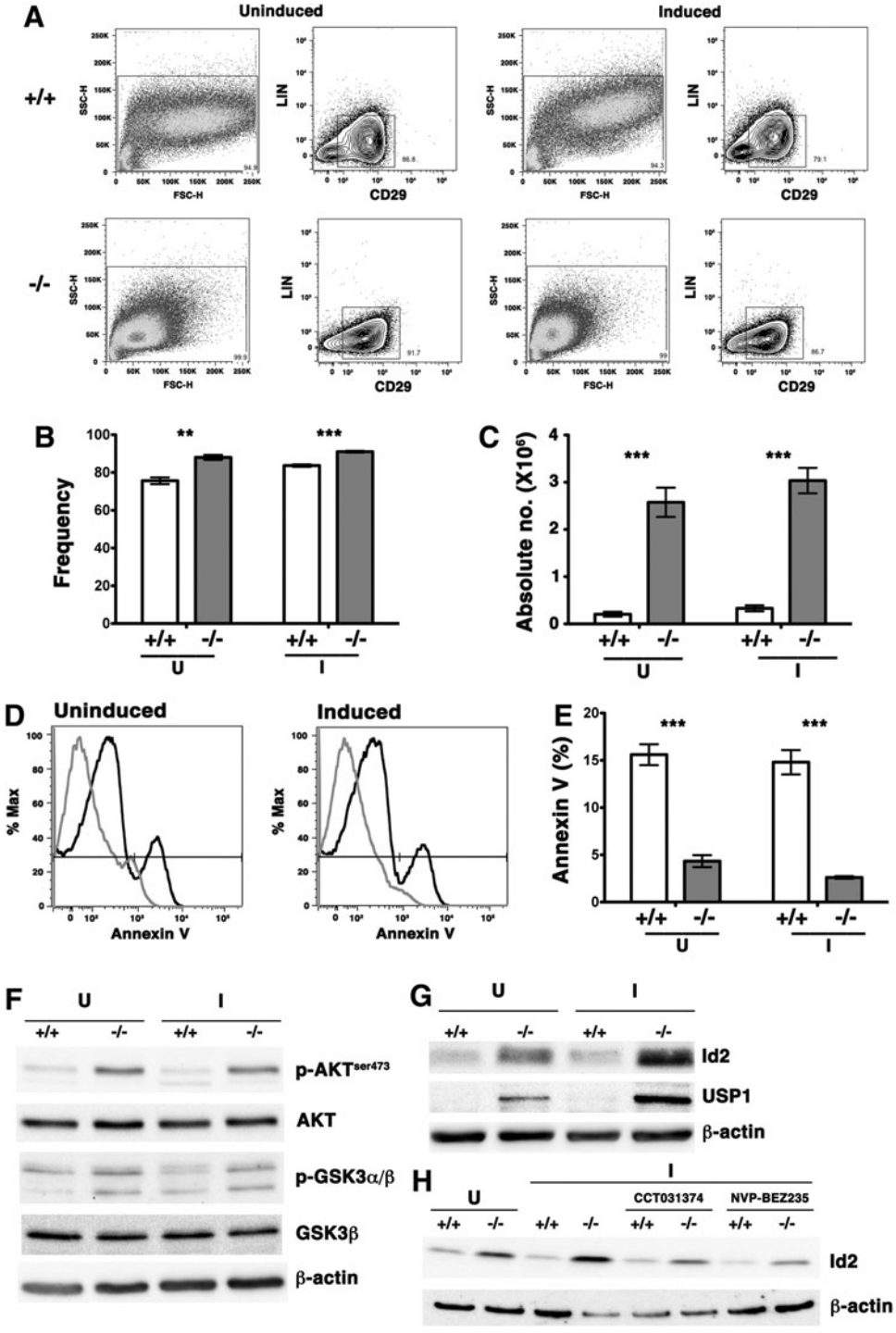

transcription factor has been shown to promote MSC proliferation, while selectively blocking osteolineage differentiation by MSCs [14,15].

To determine whether β-catenin contributes to super-induction of Id2 in OSXCreSHIP$^{flox/flox}$ MSCs we cultured SHIP1-competent SHIP$^{flox/flox}$ and OSXCreSHIP$^{flox/flox}$ MSC in the presence of a β-catenin inhibitor, CCT031374 [30]. β-catenin inhibition reduced induction of Id2 in OSXCreSHIP$^{flox/flox}$ MS/PC relative to untreated controls under osteogenic induction when Id2 level is the highest in SHIP1-deficient MSC (Fig. 4H). Using a similar approach we confirmed that PI3K pathway promotes super-induction of Id2 as a pan PI3K/mTOR inhibitor, NVP-BEZ235 [31], also reduced Id2 super-induction in OSXCreSHIP$^{flox/flox}$ MSC (Fig. 4H). These biochemical studies show that SHIP1 prevents activation of the PI3K/Akt/β-catenin signaling that can super-induce Id2 and thus promote MSC proliferation while simultaneously block their osteolineage differentiation.

SHIP1 expression in mature osteolineage cells is not required for bone formation

To further examine the functional role of SHIP1 in OBs, we crossed mice harboring floxed SHIP locus [25] with mice carrying the Cre recombinase transgene under the control of the type I collagen (Col1a1) promoter [28] to generate Col1a1CreSHIP$^{flox/flox}$ mice. The loss of SHIP1 in mature OBs in 4–6-weeks-old Col1a1CreSHIP$^{flox/flox}$ mice resulted in no effects on their growth (Fig. 5A). No difference was observed on whole body BMD and BMC by DEXA analysis in Col1a1CreSHIP$^{flox/flox}$ mice relative to SHIP$^{flox/flox}$ controls (Fig. 5B-C). MicroCT analysis showed that Col1a1CreSHIP$^{flox/flox}$ mice have normal metaphyseal Bv/Tv (Fig. 5D). In addition, we observed no difference in MS/PC frequency as defined by the PDGFRα$^+$CD51$^+$ CD31$^-$CD45$^-$Lin$^-$ phenotype [36] (Fig. 5E, F) or the PDGFRα$^+$Sca1$^+$CD31$^-$CD45$^-$Lin$^-$ phenotype [37] in Col1a1CreSHIP$^{flox/flox}$ as compared to SHIP$^{flox/flox}$ controls (Supplementary Fig. S3A, B). Because Col1a1CreSHIP$^{flox/flox}$ mice exhibit normal bone development and a normal frequency of MSC, while OSXCreSHIP$^{flox/flox}$ mice show significant alterations in both, we conclude that SHIP1 acts at the MS/PC stage and not in mature OB to influence bone development and growth in vivo.

SHIP1 expression in OCs does not limit OC differentiation and activity in vivo

A previous study suggested that germline SHIP1$^{-/-}$ mice were osteoporotic due to increased numbers of OC in vivo that were shown to be hyper-resorptive ex vivo [23]. Our collaborative study confirmed the hyper-resorptive capacity of SHIP1$^{-/-}$ OC ex vivo and attributed this to a failure of SHIP1 to block PI3K recruitment to DAP12: TREM2 complexes expressed by OC [24]. However, given our findings of osteoporosis in mice where SHIP ablation is confined to the osteolineage, we questioned whether the failure of normal bone growth and formation in SHIP$^{-/-}$

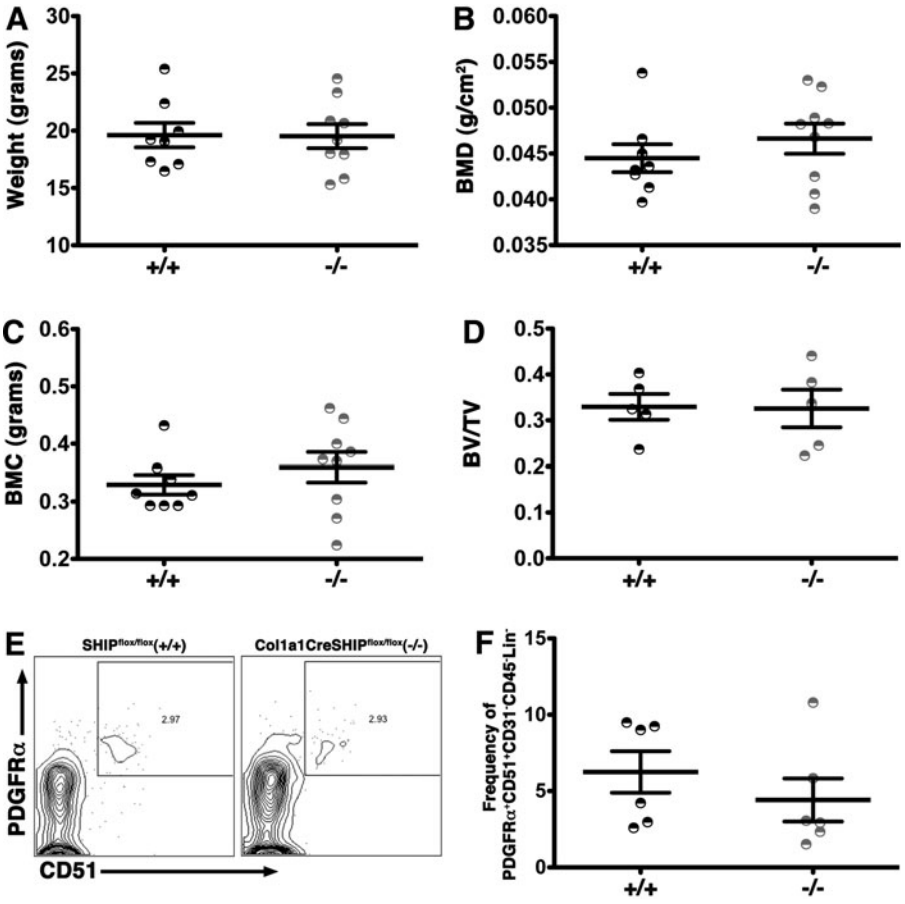

FIG. 5. SHIP1 expression in mature OBs does not limit bone apposition. No difference was observed in **(A)** body weight, **(B)** BMD, **(C)** BMC and **(D)** Bv/Tv in 4-6 week old Col1a1CreSHIP$^{flox/flox}$ (−/−) in comparison to SHIP$^{flox/flox}$ controls (+/+). No difference was observed in Pα$^+$51$^+$ MSC frequency among CD31$^-$CD45$^-$Lin$^-$ cells in 8–10-week-old SHIP$^{flox/flox}$ (+/+) and Col1a1CreSHIP$^{flox/flox}$ (−/−) mice. **(E)** Representative contour plots of PDGFRα$^+$51$^+$ MSC (PDGFRα$^+$CD51$^+$CD31$^-$ CD45$^-$Lin$^-$) and **(F)** bar graph indicating the frequency of Pα$^+$ 51$^+$ MSC in SHIP$^{flox/flox}$ (+/+) and Col1a1CreSHIP$^{flox/flox}$ (−/−) mice ($n=6$). Note: results presented for body weight, BMD, BMC, and Bv/Tv represent pooled male and female SHIP$^{flox/flox}$ and Col1a1CreSHIP$^{flox/flox}$ mice.

mice is actually a consequence of hyper-resorptive OC in vivo. As OC are a terminally differentiated myeloid lineage cell, we developed LysMCreSHIP$^{flox/flox}$ mice where myeloid-derived cells are selectively rendered SHIP1-deficient. As anticipated, this genetic strategy resulted in robust ablation of SHIP1 expression in OC from LysMCreSHIP$^{flox/flox}$ mice (Fig. 6A). However, no difference was observed in circulating monocyte numbers in LysMCreSHIP$^{flox/flox}$ and SHIP$^{flox/flox}$ controls indicating that myeloid expression of SHIP1 is not necessary to limit the size of the circulating myeloid cell compartment in vivo (Fig. 6B). We then performed detailed analysis on internal micro-architecture of 16-weeks-old adult LysMCreSHIP$^{flox/flox}$ mice using DEXA, microCT and the CFU-F assay. DEXA analysis failed to show any negative

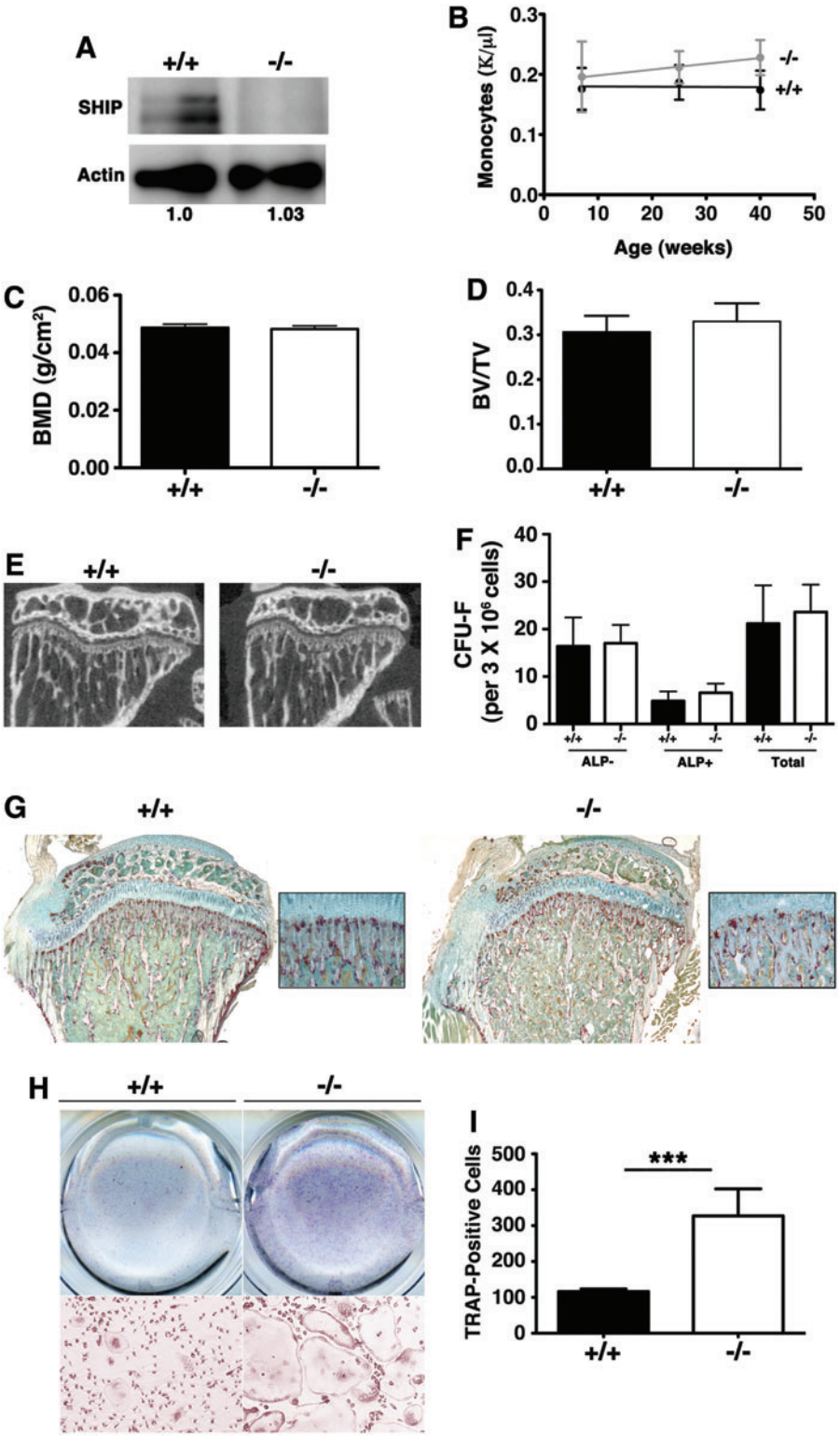

FIG. 6. A SHIP1-deficient OC compartment does not lead to osteoporosis. **(A)** Monocytes were differentiated with RANKL and M-CSF and SHIP1 levels in OC from SHIP$^{flox/flox}$ (+/+) and LysMCre-SHIP$^{flox/flox}$ (−/−) mice were assessed by western blot. Actin serves as a loading control and its relative quantification is indicated below. **(B)** Circulating monocyte in peripheral blood measured at 7, 25, and 40 weeks of age in male and female LysMCreSHIP$^{flox/flox}$ (−/−) versus SHIP$^{flox/flox}$ littermates (+/+). **(C)** Whole-body BMD by DEXA analysis, **(D)** Bv/Tv measurements and **(E)** in sagittal sections through the proximal metaphysis taken derived from microCT scans of 16-week-old male SHIP$^{flox/flox}$ (+/+) and LysMCreSHIP$^{flox/flox}$ (−/−) mice (these results are representative of four mice of each genotype). **(F)** Quantitative plots of colony forming unit-fibroblast (CFU-F) numbers (per 3×10^6 cells) from 16-week-old male SHIP$^{flox/flox}$ (+/+) (*black bars*) and LysMCreSHIP$^{flox/flox}$ (−/−) (*open bars*), mice ($n=5$). **(G)** TRAP stained proximal tibia sections of SHIP$^{flox/flox}$ (+/+) and LysMCreSHIP$^{flox/flox}$ (−/−) (4× and 20× magnification). **(H)** TRAP staining of OCs prepared from BMM that were cultured with RANKL and M-CSF showed a ∼2.8-fold increase in OC numbers in 16 weeks LysMCreSHIP$^{flox/flox}$ (−/−) versus SHIP$^{flox/flox}$ littermates (+/+). *Top panels* are representative plates and the *bottom panels* are 10×-magnified images from these plates. **(I)** The corresponding bar graphs (SHIP$^{flox/flox}$ (+/+) (*black bars*) and LysMCreSHIP$^{flox/flox}$ (−/−) (*open bars*) to the right represent mean OC numbers as determined for cultures from four mice/genotype with BMM from each mouse analyzed in duplicate (±SEM, $***P\le0.0001$, Student's unpaired, two-tailed *t*-test). Note: no significant differences were observed in BMD and Bv/Tv in female SHIP$^{flox/flox}$ and LysMCre-SHIP$^{flox/flox}$ littermates. Color images available online at www.liebertpub.com/scd

impact on whole body BMD in adult LysMCreSHIP$^{flox/flox}$ mice relative to SHIP$^{flox/flox}$ controls (Fig. 6C). MicroCT analysis also failed to show any significant difference in trabecular bone Bv/Tv (Fig. 6D). Further, microCT analysis of the tibia (Fig. 6E) revealed no difference in metaphyseal thickness in comparison to age-matched SHIP$^{flox/flox}$ controls demonstrating that a SHIP-deficient OC compartment has no negative impact on bone mass accrual in vivo. In addition, OBs are found in normal numbers in LysMCreSHIP$^{flox/flox}$ mice as we observed normal numbers of ALP^{+} colonies (Fig. 6F). TRAP staining of bone sections indicated there were normal numbers of OC present in the bone of LysMCreSHIP$^{flox/flox}$ as compared to SHIP$^{flox/flox}$ mice (Fig. 6G), but, and consistent with previous findings, [23,24] SHIP-deficient OC from LysMCreSHIP$^{flox/flox}$ expand to a greater extent when cultured ex vivo in the presence of M-CSF and receptor activator of nuclear factor kappa-B ligand (RANKL) relative to OC from SHIP$^{flox/flox}$ controls (Fig. 6H, I). Thus, a SHIP1-competent OB compartment limits the regulation of OC differentiation and resorptive behavior in vivo to prevent the development of osteoporosis. However, SHIP1 also has an OC cell autonomous role in limiting control of their response to key differentiation-inducing ligands like M-CSF and RANKL. Nonetheless, a SHIP1-deficient OC compartment is not sufficient to cause loss of bone mass or density.

Administration of a SHIPi reduces bone mass

Based on our findings in the OSXCreSHIP$^{flox/flox}$ model we hypothesized that chemical inhibition of SHIP1 might be employed as a therapeutic intervention for pathological increases in bone growth. A selective, small molecule inhibitor of SHIP1, 3AC [18,19], has recently been identified. Patients with osteopetrosis and sclerotic bone diseases present with pathologically increased bone mass, for which there are no effective therapies and thus if chemical inhibition of SHIP1 in vivo (SHIPi) can reduce bone growth then such compounds might become an effective therapy. To test the feasibility of these hypotheses, we administered the SHIPi to adult mice three times per week for 1–3 months. We find that SHIPi significantly reduces whole-body BMD (Fig. 7A) and bone mass (Fig. 7B). SHIPi treatment also resulted in diminished mechanical properties in the treated femurs; with a 15.4% ($P < 0.01$) decrease in the peak load and a 21.6% ($P < 0.04$) decrease in the stiffness (Supplementary Table S2). These changes correspond to significant decreases in cortical thickness in the femurs of SHIPi-treated mice (Supplementary Table S2). However, the energy to peak and the energy to fracture were not observed to be significantly different (Supplementary Table S2), suggesting that SHIPi-treated limbs are able to undergo similar levels of deformation prior to failure. Taken together, these data suggest that SHIPi effects are primarily through diminished bone apposition, which in an adult mouse would occur at the periosteal and endosteal surfaces and not through turnover of the metaphyseal bone. Nevertheless, it remains unclear if the relatively modest decrease in peak load and stiffness observed in the SHIPi-treated mice would incur an increase in the incidence of pathologic fracture. Taken together, these data indicate that SHIP1 inhibition may have the potential in osteopetrotic and other sclerotic bone disorders to repress unrestrained osteoblastogenesis.

Discussion

Our findings shed new light on the origin of osteoporotic pathology in SHIP1-deficient mice. We confirm the earlier findings of Takeshita et al. [23] and Peng et al. [24] that showed a cell autonomous role for SHIP in limiting the response of OC to M-CSF and RANKL ex vivo. However, our findings also demonstrate a novel role for SHIP1 in osteogenesis and indicate a SHIP-competent OB compartment regulates OC differentiation and resorptive capacity in vivo and can prevent SHIP1-deficient OCs from undergoing dysregulated differentiation and function in situ. Our findings also have potential therapeutic implications for Paget's disease, and particularly Paget kindreds where genome-wide association study (GWAS) analysis has implicated a genetic locus at 2q37—the location of the human SHIP1/INPP5D locus [52]. If human SHIP1 deficiency is found to be linked to disease in these kindreds, then our findings suggest that a hematopoietic marrow graft to replace a hyper-resorptive OC compartment may not be beneficial as the disease pathology is likely caused by SHIP1 deficiency in mesenchymal-derived OB that are not replenished from donor HSC following BMT.

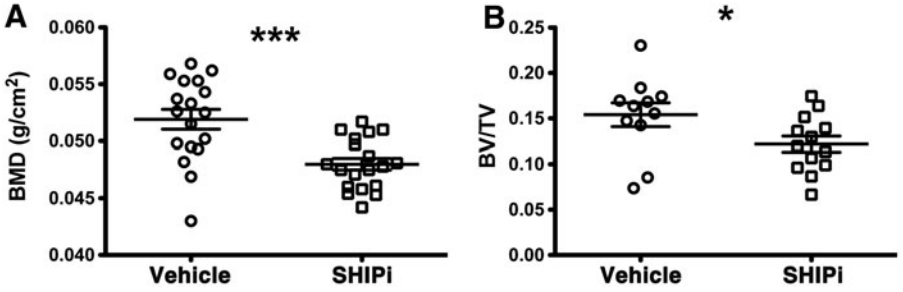

FIG. 7. SHIP1 inhibitor (SHIPi) reduces bone mass. Male 6–12-month-old C57BL6/J mice were injected intraperitoneally with vehicle or SHIPi, a SHIP1 inhibitor, at 25 mg/kg three times per week for 4, 8, and 12 weeks. Significant decrease was observed in **(A)** whole-body BMD by DEXA analysis in SHIPi-treated group (*open square*) versus vehicle group (*open circle*) ($\pm$SEM ***$P \leq 0.0001$ Student's unpaired, two-tailed *t*-test). **(B)** Metaphyseal histomorphometric parameter, Bv/Tv was significantly decreased after SHIPi treatment in the SHIPi group (*open squares*) in comparison to vehicle group (*open circles*) ($\pm$SEM *$P \leq 0.05$ Student's unpaired, two-tailed *t*-test, each symbol represents an individual mouse).

Chen et al. have recently shown that activation of a ROSA-stop-flox reporter in all MSC-derived marrow cell types in postnatal mice including stromal cells, adipocytes, and perivascular lining cells [41]. Consistent with their elegant demonstration of OSXCre-mediated gene deletion in MSC-derived lineages, here we have demonstrated ablation of SHIP1 expression MSCs derived from OSXCreSHIP$^{flox/flox}$ mice. The growth plate chondrocyte defect that we also observe in the OSXCreSHIP$^{flox/flox}$ mice might potentially reflect a requirement for SHIP1 by MSC for their efficient commitment to the chondrocyte lineage, much like we observe with osteolineage cells. However, it might also reflect a requirement for SHIP1 expression within the chondrocyte lineage for their terminal maturation. In addition, longitudinal growth deficiency we observe might also be associated with a loss of chondrocyte hypertrophy and the corresponding loss of chondrocyte terminal differentiation [53]. Terminal differentiation in hypertrophic chondrocytes is required to efficiently attract osteoprogenitors and OC precursors; therefore, it is possible that some of the effects observed on bone formation and bone resorption in OSX-CreSHIP$^{flox/flox}$ mice are due to a loss of chondrocyte hypertrophy.

The osteoblastic requirement for SHIP1 that we have identified here represents the first function demonstrated for SHIP1 in a cell type that is not a component of the hematolymphoid compartment. As SHIP1 is not typically expressed in mesenchymal lineages its expression could potentially be controlled by transcription factors active in both hematopoietic and mesenchymal lineages. In this regard, a potential candidate regulator is SMAD4, which is required for OB development [54] and known to also induce expression of SHIP1 in myeloid cells [55]. Induction of SHIP1 by SMAD4 may in turn repress the activity of other SMAD factors that promote stemness and MSC proliferation (eg, USP1, Id2). Since the deletion of SHIP1 in Col1a1-CreSHIP$^{flox/flox}$ mice is restricted to mature OB and not MSC, these data further support the observation in the OSXCreSHIP$^{flox/flox}$ mice that SHIP1 expression is required for efficient OB differentiation from MSC.

Our findings implicate SHIP1 at the nexus of a novel molecular pathway that limits Id2 expression, and consequently MSC proliferation, while also promoting commitment of MSC to osteolineage development. Williams et al. [15] identified USP1 and its co-factor WDR48 in MSC and as such are potential targets for SHIP1 regulation in MSC. Our findings demonstrate that SHIP1 expression in MSC limits USP1 expression and consequently Id2 expression. Park et al. demonstrated that super-physiological expression of Id2 promotes adipocyte differentiation by promoting PPARγ activity in adipocyte progenitors [56]. Thus, increased expression of Id2 in SHIP1-deficient MSCs corresponds with reduced OB differentiation and increased adipogenesis that we observed in vivo in OSXCreSHIP$^{flox/flox}$ mice and in MSC ex vivo. By heterodimerizing with bHLH proteins (eg, MyoD) Id proteins antagonize differentiation of stem/progenitor cells and also drive the G1/S cell cycle transition in these primitive cells [57,58]. Indeed, Id2 has been found to promote self-renewal or cycling of MSC, HSC and neural stem cells [15,51,59–61]. Moreover, enforced expression of Id2 suppresses OB differentiation by MSC [14].

Our findings are the first to show that SHIP1 can promote lineage commitment in a population of MS/PC rather than simply acting as an inhibitor of cell survival and function in differentiated cells. Due to its essential role in cell survival, the PI3K/Akt pathway and inositol phosphatases that regulate it are proposed to play a role in stem cell self-renewal, maintenance, and differentiation. This includes several types of stem cells, including pluripotent stem cells, [31,62–65] HSC, [20,22,66–68] neural stem cells [69–74], and epithelial stem cells [75]. A recurring theme in several stem cell types is for the PI3K/Akt pathway to inactivate GSK3β thus promoting activation and nuclear translocation of β-catenin [76,77]. Our studies suggest a similar role for this pathway in MS/PCs that is regulated by SHIP1. Our study also identifies a SHIP1 regulated switch that controls the USP1/WDR48/Id2 axis that promotes stemness versus lineage commitment in MSC.

We administered SHIPi to adult mice and found that this could selectively reduce bone mass, without producing a significant loss in mechanical properties or bone morphology. Osteopetrosis is a collection of intractable and incurable syndromes that manifest as a pathologic increase in bone mass [78]. Sclerotic bone diseases are often treated surgically and have a poor long-term prognosis, often leading to fracture and disunion [79]. In this context SHIPi may represent an effective adjuvant chemotherapeutic. SHIPi may represent a novel therapy for these conditions for which there is currently no known pharmacological intervention.

Acknowledgments

This work was supported in part by grants from the NIH (RO1 HL72523, R01 HL085580, and R01 HL107127) and the Paige Arnold Butterfly Run. W.G.K. is the Murphy Family Professor of Children's Oncology Research, an Empire Scholar of the State University of NY, and a Senior Scholar of the Crohn's and Colitis Foundation of America.

Author Disclosure Statement

W.G.K., J.D.C., and S.I. have patents, pending and issued, concerning the analysis and targeting of SHIP1 in disease. The other authors have no conflicts to disclose and no competing financial interests exist.

References

1. Hadjidakis DJ and I Androulakis. (2006). Bone remodeling. Ann N Y Acad Sci 1092:385–396.
2. Friedenstein AJ, KV Petrakova, AI Kurolesova and GP Frolova. (1968). Heterotopic of bone marrow. Analysis of precursor cells for osteogenic and hematopoietic tissues. Transplantation 6:230–247.
3. Friedenstein AJ, UF Deriglasova, NN Kulagina, AF Panasuk, SF Rudakowa, EA Luria and IA Ruadkow. (1974). Precursors for fibroblasts in different populations of hematopoietic cells as detected by the in vitro colony assay method. Exp Hematol 2:83–92.
4. Owen M and AJ Friedenstein. (1988). Stromal stem cells: marrow-derived osteogenic precursors. Ciba Found Symp 136:42–60.
5. Caplan AI. (1991). Mesenchymal stem cells. J Orthop Res 9:641–650.

6. Mendez-Ferrer S, TV Michurina, F Ferraro, AR Mazloom, BD Macarthur, SA Lira, DT Scadden, A Ma'ayan, GN Enikolopov and PS Frenette. (2010). Mesenchymal and haematopoietic stem cells form a unique bone marrow niche. Nature 466:829–834.
7. Bianco P, PG Robey and PJ Simmons. (2008). Mesenchymal stem cells: revisiting history, concepts, and assays. Cell Stem Cell 2:313–319.
8. Massari ME and C Murre. (2000). Helix-loop-helix proteins: regulators of transcription in eucaryotic organisms. Mol Cell Biol 20:429–440.
9. Benezra R, RL Davis, D Lockshon, DL Turner and H Weintraub. (1990). The protein Id: a negative regulator of helix-loop-helix DNA binding proteins. Cell 61:49–59.
10. O'Toole PJ, T Inoue, L Emerson, IE Morrison, AR Mackie, RJ Cherry and JD Norton. (2003). Id proteins negatively regulate basic helix-loop-helix transcription factor function by disrupting subnuclear compartmentalization. J Biol Chem 278:45770–45776.
11. Jogi A, P Persson, A Grynfeld, S Pahlman and H Axelson. (2002). Modulation of basic helix-loop-helix transcription complex formation by Id proteins during neuronal differentiation. J Biol Chem 277:9118–9126.
12. Lasorella A, T Uo and A Iavarone. (2001). Id proteins at the cross-road of development and cancer. Oncogene 20:8326–8333.
13. Zebedee Z and E Hara. (2001). Id proteins in cell cycle control and cellular senescence. Oncogene 20:8317–8325.
14. Peng Y, Q Kang, Q Luo, W Jiang, W Si, BA Liu, HH Luu, JK Park, X Li, et al. (2004). Inhibitor of DNA binding/differentiation helix-loop-helix proteins mediate bone morphogenetic protein-induced osteoblast differentiation of mesenchymal stem cells. J Biol Chem 279: 32941–32949.
15. Williams SA, HL Maecker, DM French, J Liu, A Gregg, LB Silverstein, TC Cao, RA Carano and VM Dixit. (2011). USP1 deubiquitinates ID proteins to preserve a mesenchymal stem cell program in osteosarcoma. Cell 146:918–930.
16. Franke TF, DR Kaplan, LC Cantley and A Toker. (1997). Direct regulation of the Akt proto-oncogene product by phosphatidylinositol-3,4-bisphosphate [see comments]. Science 275:665–668.
17. Ma K, SM Cheung, AJ Marshall and V Duronio. (2008). PI(3,4,5)P3 and PI(3,4)P2 levels correlate with PKB/akt phosphorylation at Thr308 and Ser473, respectively; PI(3,4)P2 levels determine PKB activity. Cell Signal 20: 684–694.
18. Brooks R, GM Fuhler, S Iyer, MJ Smith, MY Park, KH Paraiso, RW Engelman and WG Kerr. (2010). SHIP1 inhibition increases immunoregulatory capacity and triggers apoptosis of hematopoietic cancer cells. J Immunol 184: 3582–3589.
19. Fuhler GM, R Brooks, B Toms, S Iyer, EA Gengo, MY Park, M Gumbleton, DR Viernes, JD Chisholm and WG Kerr. (2012). Therapeutic potential of SH2 domain-containing inositol-5′-phosphatase 1 (SHIP1) and SHIP2 inhibition in cancer. Mol Med 18:65–75.
20. Desponts C, AL Hazen, KH Paraiso and WG Kerr. (2006). SHIP deficiency enhances HSC proliferation and survival but compromises homing and repopulation. Blood 107: 4338–4345.
21. Helgason CD, J Antonchuk, C Bodner and RK Humphries. (2003). Homeostasis and regeneration of the hematopoietic stem cell pool are altered in SHIP-deficient mice. Blood 102:3541–3547.
22. Hazen AL, MJ Smith, C Desponts, O Winter, K Moser and WG Kerr. (2009). SHIP is required for a functional hematopoietic stem cell niche. Blood 113:2924–2933.
23. Takeshita S, N Namba, JJ Zhao, Y Jiang, HK Genant, MJ Silva, MD Brodt, CD Helgason, J Kalesnikoff, et al. (2002). SHIP-deficient mice are severely osteoporotic due to increased numbers of hyper-resorptive osteoclasts. Nat Med 8:943–949.
24. Peng Q, S Malhotra, JA Torchia, WG Kerr, KM Coggeshall and MB Humphrey. (2010). TREM2- and DAP12-dependent activation of PI3K requires DAP10 and is inhibited by SHIP1. Sci Signal 3:ra38.
25. Wang JW, JM Howson, T Ghansah, C Desponts, JM Ninos, SL May, KH Nguyen, N Toyama-Sorimachi and WG Kerr. (2002). Influence of SHIP on the NK repertoire and allogeneic bone marrow transplantation. Science 295:2094–2097.
26. Rodda SJ and AP McMahon. (2006). Distinct roles for Hedgehog and canonical Wnt signaling in specification, differentiation and maintenance of osteoblast progenitors. Development 133:3231–3244.
27. Clausen BE, C Burkhardt, W Reith, R Renkawitz and I Forster. (1999). Conditional gene targeting in macrophages and granulocytes using LysMcre mice. Transgenic Res 8:265–277.
28. Dacquin R, M Starbuck, T Schinke and G Karsenty. (2002). Mouse alpha1(I)-collagen promoter is the best known promoter to drive efficient Cre recombinase expression in osteoblast. Dev Dyn 224:245–251.
29. Margulies BS, TA Damron and MJ Allen. (2008). The differential effects of the radioprotectant drugs amifostine and sodium selenite treatment in combination with radiation therapy on constituent bone cells, Ewing's sarcoma of bone tumor cells, and rhabdomyosarcoma tumor cells in vitro. J Orthop Res 26:1512–1519.
30. Ewan K, B Pajak, M Stubbs, H Todd, O Barbeau, C Quevedo, H Botfield, R Young, R Ruddle, et al. (2010). A useful approach to identify novel small-molecule inhibitors of Wnt-dependent transcription. Cancer Res 70:5963–5973.
31. Maira SM, F Stauffer, J Brueggen, P Furet, C Schnell, C Fritsch, S Brachmann, P Chene, A De Pover, et al. (2008). Identification and characterization of NVP-BEZ235, a new orally available dual phosphatidylinositol 3-kinase/mammalian target of rapamycin inhibitor with potent in vivo antitumor activity. Mol Cancer Ther 7:1851–1863.
32. Margulies BS, JA Horton, Y Wang, TA Damron and MJ Allen. (2006). Effects of radiation therapy on chondrocytes in vitro. Calcif Tissue Int 78:302–313.
33. Cruz-Orive LM and ER Weibel. (1990). Recent stereological methods for cell biology: a brief survey. Am J Physiol 258:L148–L156.
34. Margulies B, H Morgan, M Allen, J Strauss, J Spadaro and T Damron. (2003). Transiently increased bone density after irradiation and the radioprotectant drug amifostine in a rat model. Am J Clin Oncol 26:e106–e114.
35. Damron TA, BS Margulies, JA Strauss, K O'Hara, JA Spadaro and CE Farnum. (2003). Sequential histomorphometric analysis of the growth plate following irradiation with and without radioprotection. J Bone Joint Surg Am 85-A:1302–1313.
36. Pinho S, J Lacombe, M Hanoun, T Mizoguchi, I Bruns, Y Kunisaki and PS Frenette. (2013). PDGFRalpha and CD51

mark human nestin+sphere-forming mesenchymal stem cells capable of hematopoietic progenitor cell expansion. J Exp Med 210:1351–1367.
37. Morikawa S, Y Mabuchi, Y Kubota, Y Nagai, K Niibe, E Hiratsu, S Suzuki, C Miyauchi-Hara, N Nagoshi, et al. (2009). Prospective identification, isolation, and systemic transplantation of multipotent mesenchymal stem cells in murine bone marrow. J Exp Med 206:2483–2496.
38. Winkler IG, V Barbier, R Wadley, AC Zannettino, S Williams and JP Levesque. (2010). Positioning of bone marrow hematopoietic and stromal cells relative to blood flow in vivo: serially reconstituting hematopoietic stem cells reside in distinct nonperfused niches. Blood 116:375–385.
39. Schepers K, EC Hsiao, T Garg, MJ Scott and E Passegue. (2012). Activated Gs signaling in osteoblastic cells alters the hematopoietic stem cell niche in mice. Blood 120:3425–3435.
40. Houlihan DD, Y Mabuchi, S Morikawa, K Niibe, D Araki, S Suzuki, H Okano and Y Matsuzaki. (2012). Isolation of mouse mesenchymal stem cells on the basis of expression of Sca-1 and PDGFR-alpha. Nat Protoc 7:2103–2111.
41. Chen J, Y Shi, J Regan, K Karuppaiah, DM Ornitz and F Long. (2014). Osx-Cre targets multiple cell types besides osteoblast lineage in postnatal mice. PLoS One 9:e85161.
42. Wilsman NJ, CE Farnum, EM Leiferman, M Fry and C Barreto. (1996). Differential growth by growth plates as a function of multiple parameters of chondrocytic kinetics. J Orthop Res 14:927–936.
43. Pateder DB, RN Rosier, EM Schwarz, PR Reynolds, JE Puzas, M D'Souza and RJ O'Keefe. (2000). PTHrP expression in chondrocytes, regulation by TGF-beta, and interactions between epiphyseal and growth plate chondrocytes. Exp Cell Res 256:555–562.
44. Chung UI, E Schipani, AP McMahon and HM Kronenberg. (2001). Indian hedgehog couples chondrogenesis to osteogenesis in endochondral bone development. J Clin Invest 107:295–304.
45. Collazo MM, KHT Paraiso, M-Y Park, AL Hazen and WG Kerr. (2012). Lineage extrinsic and intrinsic control of immunoregulatory cell numbers by SHIP. Eur J Immunol 42: 1785–1795.
46. Yamashita T, N Takahashi and N Udagawa. (2012). New roles of osteoblasts involved in osteoclast differentiation. World J Orthop 3:175–181.
47. Martin TJ and KW Ng. (1994). Mechanisms by which cells of the osteoblast lineage control osteoclast formation and activity. J Cell Biochem 56:357–366.
48. Marcus R, D Feldman, D Nelson and CJ Rosen. (2009). *Fundamentals of Osteoporosis*. Elsevier Science, Waltham.
49. Teitelbaum SL and FP Ross. (2003). Genetic regulation of osteoclast development and function. Nat Rev Genet 4:638–649.
50. Zhu H, ZK Guo, XX Jiang, H Li, XY Wang, HY Yao, Y Zhang and N Mao. (2010). A protocol for isolation and culture of mesenchymal stem cells from mouse compact bone. Nat Protoc 5:550–560.
51. Perry JM, XC He, R Sugimura, JC Grindley, JS Haug, S Ding and L Li. (2011). Cooperation between both Wnt/{beta}-catenin and PTEN/PI3K/Akt signaling promotes primitive hematopoietic stem cell self-renewal and expansion. Genes Dev 25:1928–1942.
52. Hocking LJ, CA Herbert, RK Nicholls, F Williams, ST Bennett, T Cundy, GC Nicholson, W Wuyts, W Van Hul and SH Ralston. (2001). Genomewide search in familial Paget disease of bone shows evidence of genetic heterogeneity with candidate loci on chromosomes 2q36, 10p13, and 5q35. Am J Hum Genet 69:1055–1061.
53. Kronenberg HM. (2003). Developmental regulation of the growth plate. Nature 423:332–336.
54. Tan X, T Weng, J Zhang, J Wang, W Li, H Wan, Y Lan, X Cheng, N Hou, et al. (2007). Smad4 is required for maintaining normal murine postnatal bone homeostasis. J Cell Sci 120:2162–2170.
55. Pan H, E Ding, M Hu, AS Lagoo, MB Datto and SA Lagoo-Deenadayalan. (2010). SMAD4 is required for development of maximal endotoxin tolerance. J Immunol 184: 5502–5509.
56. Park KW, H Waki, CJ Villanueva, LA Monticelli, C Hong, S Kang, OA MacDougald, AW Goldrath and P Tontonoz. (2008). Inhibitor of DNA binding 2 is a small molecule-inducible modulator of peroxisome proliferator-activated receptor-gamma expression and adipocyte differentiation. Mol Endocrinol 22:2038–2048.
57. Norton JD. (2000). ID helix-loop-helix proteins in cell growth, differentiation and tumorigenesis. J Cell Sci 113 (Pt 22):3897–3905.
58. Norton JD, RW Deed, G Craggs and F Sablitzky. (1998). Id helix-loop-helix proteins in cell growth and differentiation. Trends Cell Biol 8:58–65.
59. Jung S, RH Park, S Kim, YJ Jeon, DS Ham, MY Jung, SS Kim, YD Lee, CH Park and H Suh-Kim. (2010). Id proteins facilitate self-renewal and proliferation of neural stem cells. Stem Cells Dev 19:831–841.
60. Li H, M Ji, KD Klarmann and JR Keller. (2010). Repression of Id2 expression by Gfi-1 is required for B-cell and myeloid development. Blood 116:1060–1069.
61. Paolella BR, MC Havrda, A Mantani, CM Wray, Z Zhang and MA Israel. (2011). p53 directly represses Id2 to inhibit the proliferation of neural progenitor cells. Stem Cells 29: 1090–1101.
62. Kroger N, R Brand, A van Biezen, JY Cahn, S Slavin, D Blaise, J Sierra, A Zander, D Niederwieser and T de Witte. (2006). Autologous stem cell transplantation for therapy-related acute myeloid leukemia and myelodysplastic syndrome. Bone Marrow Transplant 37:183–189.
63. Welham MJ, MP Storm, E Kingham and HK Bone. (2007). Phosphoinositide 3-kinases and regulation of embryonic stem cell fate. Biochem Soc Trans 35:225–228.
64. Wang H, P Zhang, L Liu and L Zou. (2013). Hierarchical organization and regulation of the hematopoietic stem cell osteoblastic niche. Crit Rev Oncol Hematol 85:1–8.
65. Yoon KA, HS Cho, HI Shin and JY Cho. (2012). Differential regulation of CXCL5 by FGF2 in osteoblastic and endothelial niche cells supports hematopoietic stem cell migration. Stem Cells Dev 21:3391–3402.
66. Tu Z, JM Ninos, Z Ma, JW Wang, MP Lemos, C Desponts, T Ghansah, JM Howson and WG Kerr. (2001). Embryonic and hematopoietic stem cells express a novel SH2-containing inositol 5′-phosphatase isoform that partners with the Grb2 adapter protein. Blood 98:2028–2038.
67. Yilmaz OH, R Valdez, BK Theisen, W Guo, DO Ferguson, H Wu and SJ Morrison. (2006). Pten dependence distinguishes haematopoietic stem cells from leukaemia-initiating cells. Nature 441:475–482.
68. Zhang J, JC Grindley, T Yin, S Jayasinghe, XC He, JT Ross, JS Haug, D Rupp, KS Porter-Westpfahl, et al. (2006). PTEN maintains haematopoietic stem cells and acts in lineage choice and leukaemia prevention. Nature 441:518–522.

69. Chell JM and AH Brand. (2010). Nutrition-responsive glia control exit of neural stem cells from quiescence. Cell 143:1161–1173.
70. Le Belle JE, NM Orozco, AA Paucar, JP Saxe, J Mottahedeh, AD Pyle, H Wu and HI Kornblum. (2011). Proliferative neural stem cells have high endogenous ROS levels that regulate self-renewal and neurogenesis in a PI3K/Akt-dependant manner. Cell Stem Cell 8:59–71.
71. Paik J-h, Z Ding, R Narurkar, S Ramkissoon, F Muller, WS Kamoun, S-S Chae, H Zheng, H Ying, et al. (2009). FoxOs cooperatively regulate diverse pathways governing neural stem cell homeostasis. Cell Stem Cell 5:540–553.
72. Zhang Q, G Liu, Y Wu, H Sha, P Zhang and J Jia. (2011). BDNF promotes EGF-induced proliferation and migration of human fetal neural stem/progenitor cells via the PI3K/Akt pathway. Molecules 16:10146–10156.
73. Ojeda L, J Gao, KG Hooten, E Wang, JR Thonhoff, TJ Dunn, T Gao and P Wu. (2011). Critical role of PI3K/Akt/GSK3β in motoneuron specification from human neural stem cells in response to FGF2 and EGF. PLoS One 6: e23414.
74. Groszer M, R Erickson, DD Scripture-Adams, R Lesche, A Trumpp, JA Zack, HI Kornblum, X Liu and H Wu. (2001). Negative regulation of neural stem/progenitor cell proliferation by the Pten tumor suppressor gene in vivo. Science 294:2186–2189.
75. Sewell GW, DJ Marks and AW Segal. (2009). The immunopathogenesis of Crohn's disease: a three-stage model. Curr Opin Immunol 21:506–513.
76. Bechard M, R Trost, Singh AM, Dalton S. (2012). Frat is a phosphatidylinositol 3-kinase/Akt-regulated determinant of glycogen synthase kinase 3β subcellular localization in pluripotent cells. Mol Cell Biol 32:288–296.
77. Korkaya H, A Paulson, Charafe-Jauffret E, Ginestier C, Brown M, Dutcher J, Clouthier SG, Wicha MS. (2009). Regulation of mammary stem/progenitor cells by PTEN/Akt/beta-catenin signaling. PLoS Biol 7:e1000121.
78. Whyte MP and Asbmr. (2009). Chapter 88. Sclerosing bone disorders. In: *Primer on the Metabolic Bone Diseases and Disorders of Mineral Metabolism*. John Wiley & Sons, Inc., Hoboken, NJ, pp 411–423.
79. Wall JE, SC Kaste, CA Greenwald, JJ Jenkins, EC Douglass and CB Pratt. (1996). Fractures in children treated with radiotherapy for soft tissue sarcoma. Orthopedics 19:657–664.

Address correspondence to:
Dr. William G. Kerr
Department of Microbiology and Immunology
SUNY Upstate Medical University
Syracuse, NY 13210

E-mail: kerrw@upstate.edu

Received for publication March 7, 2014
Accepted after revision May 22, 2014
Prepublished on Liebert Instant Online May 24, 2014